Agricultural and Forest Meteorology 249 (2018) 310–318

Contents lists available at ScienceDirect

Agricultural and Forest Meteorology

journal homepage: www.elsevier.com/locate/agrformet

Modeling spatiotemporal variations in leaf coloring date of three tree species across China

Zexing Tao[a,b], Huanjiong Wang[a], Junhu Dai[a,b,*], Juha Alatalo[c], Quansheng Ge[a,*]

[a] Key Laboratory of Land Surface Pattern and Simulation, Institute of Geographic Sciences and Natural Resources Research, Chinese Academy of Sciences, Beijing 100101, China

[b] University of Chinese Academy of Sciences, Beijing 100049, China

[c] Department of Biological and Environmental Sciences, College of Arts and Sciences, Qatar University, P.O. Box 2713, Doha, Qatar

ARTICLE INFO

Keywords:
Autumn phenology
Modeling
Leaf coloring date
Empirical orthogonal function

ABSTRACT

Autumn phenology can regulate climate-biosphere interactions and net primary production within the ecosystem. However, studies modeling spatiotemporal variations in leaf coloring date (LCD) remain limited, especially for species-specific phenology on a continental scale. Aiming to simulate spatiotemporal variations in LCD in three widespread tree species (*Ulmus pumila*, *Fraxinus chinensis,* and *Robinia pseudoacacia*) across China, we used phenological observation records acquired from the China Phenology Observation Network (CPON) during 1963–2010 to establish and compare three LCD models (multiple regression (MA), temperature-photoperiod (TP), spring-influenced autumn (SIA)). Subsequently, we simulated the mean LCD of the three species using the most effective model and examined the effect of geographical factors (i.e., latitude, longitude, and altitude) on LCD through multiple regression analysis. Empirical Orthogonal Function (EOF) analysis was applied to identifying the most extensive and influential spatial modes of LCD variability and how they changed with time. The results showed that: (1) The LCD of *F. chinensis* was fitted better with the statistical model using monthly temperature as the independent variables (MR model). The LCD of *F. chinensis* was delayed by a temperature rise in August and September, but advanced by a temperature rise in May and June. The LCD of *U. pumila* and *R. pseudoacacia* was fitted better with the TP and SIA models, in which the photoperiod determined the date when the cold temperature started to accumulate. (2) The simulated mean LCD of *U. pumila*, *F. chinensis,* and *R. pseudoacacia* was October 6, October 16 and October 22, respectively. Latitude, longitude, and altitude had a significant influence on mean LCD of the three tree species. With increasing latitude and altitude, the LCD of all three species became earlier. However, the impact of longitude on the mean LCD varied among species. (3) For all the three species, the first EOF mode presented a consistent pattern of LCD variability across space, suggesting that an earlier or later LCD occurred simultaneously in the whole China. Meanwhile, the second EOF mode exhibited contrary signals of LCD variability in the north and south for *F. chinensis* and *R. pseudoacacia*. Over the past 50 years, the LCD of all the three species has delayed. The delaying trend revealed by the first EOF mode was 1.25 ($p < 0.01$), 0.21 ($p < 0.01$), and 0.53 days/decade (not significant) for *U. pumila*, *F. chinensis* and *R. pseudoacacia*, respectively. These results provide the basis for a better understanding of the phenology process in autumn and how it responds to climate change.

1. Introduction

Phenological changes have dramatic effects on carbon balance, nutrient cycles, biodiversity and net primary production in ecosystems (Cleland et al., 2007; Ge et al., 2014b), and control many feedbacks of the climate system (Ge et al., 2014a; Richardson et al., 2013). Several studies have concluded that autumn phenology might have a greater effect than spring phenology on the extension of growing season length (Garonna et al., 2014; Liu et al., 2016b) and changes in net ecosystem productivity (Wu et al., 2013). Thus, a comprehensive understanding of spatiotemporal patterns of autumn phenology could help understand structure and function of the ecosystem in autumn and to predict future ecosystem dynamics.

Phenological models play a critical role in quantifying climate-biosphere interactions (Visser, 2016; Xin, 2016). Through phenological models and meteorological data, the phenophases and their spatiotemporal patterns could be simulated accurately (Aono and Omoto, 1990; Bluemel and Chmielewski, 2012; Chuine, 2000). Compared with

* Corresponding authors.
E-mail addresses: daijh@igsnrr.ac.cn (J. Dai), geqs@igsnrr.ac.cn (Q. Ge).

https://doi.org/10.1016/j.agrformet.2017.10.034
Received 3 July 2017; Received in revised form 23 October 2017; Accepted 31 October 2017
Available online 14 November 2017
0168-1923/

spring phenological models, models regarding autumn phenology remain limited, mainly due to lack of knowledge about the phenology process and its mechanism (Olsson and Jonsson, 2015). Many external environmental factors, such as temperature, drought, ozone, nutrient deficiency, and pathogen infection, may have considerable influences on the autumn phenology process (Lim et al., 2007), and the influences may differ across species and ecosystems (Gill et al., 2015). Therefore, existing autumn phenology models based either on observations of individual trees or remote sensing have different parametric equations (Jeong and Medvigy, 2014).

The existed autumn phenological models are mostly set up according to several main influencing factors. A great number of studies put forward that temperature is the most important factor impacting autumn phenology (Chen and Xu, 2012; Ge et al., 2015; Menzel, 2003), because cold temperature may lead to water freezing in leaves and force deciduous trees to shed their leaves to prevent damage (Jeong and Medvigy, 2014). However, the start date of leaf coloring is determined by a specific threshold of minimum temperature (Estrella and Menzel, 2006) or accumulated cold temperature (Yu et al., 2016) according to different hypotheses. Photoperiod is another factor influencing autumn phenology (Fracheboud et al., 2009), especially in regions at high latitudes (Gill et al., 2015; Way and Montgomery, 2015), which can affect the formation of leaf abscission meristems and the ability of plants to tolerate low temperature (Korner and Basler, 2010). Moreover, precipitation may improve soil moisture content and change the photosynthetic efficiency by affecting the plant carboxylation reaction, and further lead to shifts in autumn phenology (Zu and Yang, 2016). Recently, spring phenology has been found to exert a significant influence on the timing of autumn phenology (Fu et al., 2014; Liu et al., 2016a), and is considered in a recent phenological model (Keenan and Richardson, 2015).

To date, many autumn phenological models are developed on the basis of few data from limited sites (Jeong et al., 2013). Thus, the established models may have great errors when simulating phenology in broad geographical regions (Basler, 2016; Delpierre et al., 2009). Several studies have made systematic comparisons among various autumn phenology models in Europe (Olsson and Jonsson, 2015) and America (Jeong and Medvigy, 2014), and have found that temperature and photoperiod can explain the variation in autumn phenology for most species, but that the parameters may vary greatly among species. However, no previous study has focused on the species-specific autumn phenology model up to date in China.

In order to compensate the above shortage and fill this knowledge gap, this study used three phenology models for simulating leaf coloring date (LCD) of three cosmopolite tree species (*Ulmus pumila*, *Fraxinus chinensis*, and *Robinia pseudoacacia*) across a large part of China. Based on the optimal model, we simulated the LCD variations in the three species over the past 50 years and analyzed their spatiotemporal patterns through empirical orthogonal function (EOF) analysis. The overall aim of the study was to explore the spatiotemporal pattern of autumn phenological change in typical species in China and try to discuss the mechanism of autumn phenology process in response to climate change.

2. Materials and methods

2.1. Data source

The three plant species (*U. pumila*, *F. chinensis,* and *R. pseudoacacia*), selected for study all have strong tolerance to severe environments, such as drought conditions and alkaline or saline soils (Solla et al., 2005; Wu et al., 1994). These species are widespread and can reflect the autumn phenological changes over large regions in China. Data on the distribution of *U. pumila* and *F. chinensis* (Fig. 1) were obtained from the Atlas of Woody Plants in China (Fang et al., 2009). The distribution of *R. pseudoacacia* in China was determined according to the Flora of China (Wu et al., 1994) and Chinese Virtual Herbarium (CVH, www.cvh.ac.cn).

The LCD data of the three species were obtained from China Phenological Observation Network (CPON) (Table A.1–A.3), which were mainly observed at sites located in eastern China (Fig. 1). The LCD for an individual tree was defined as the date when 99% of its leaves had visibly changed color. The phenological observations were interrupted during several periods (Fig. 2), so the average number of records per year was 8.6, 8.2, and 9.7 for *U. pumila*, *F. chinensis,* and *R. pseudoacacia*, respectively.

The meteorological data were downloaded from the China meteorological data service center (http://data.cma.cn/). For fitting the phenology model, we used daily air temperature data obtained near CPON sites from 1963 to 2010. For LCD simulation, we utilized a gridded dataset of daily surface air temperature at 0.5° × 0.5° resolution during 1961–2012. This dataset was generated by interpolating the data from 2472 meteorological stations using ANUSPLIN software and thin plate spline method.

2.2. Methods

2.2.1. Model calibration and validation

Three autumn models were applied to simulate the LCD. The first one was a multiple regression (MR) model. Estrella and Menzel (2006) found that LCD was delayed by a temperature rise in August and September but advanced by a temperature rise in May and June. Based on this empirical relationship, the MR model was built as a multiple linear regression function between autumn phenophase and monthly temperature:

$$P_l = aT_5 + bT_6 + cT_7 + dT_8 + eT_9 + \varepsilon \quad (1)$$

where a, b, c, d, and e are model parameters, T_5, T_6, T_7, T_8, and T_9 are the mean temperature in May, June, July, August, and September, respectively, and ε is a constant term.

The second model was a process-based model based on temperature and photoperiod (TP model), which defines a coloring state $CDD(d)$ for each day to depict the progress of leaf coloring (Delpierre et al., 2009). In the TP model, $CDD(d)$ is determined by accumulated cold temperatures and regulated by daily photoperiod [Eq. (3)]. For some species, the photoperiod not only decides the date when cold temperatures begin to accumulate [Eq. (2)], but also influences the cold degree sum effect [Eq. (4)]. The combined effect of temperature and photoperiod is shown as:

$$iCDD(d) = \begin{cases} 0 & \mathrm{P(d)} \geq P_{start} \\ \mathrm{CDD(d-1) + CDD(d)} & \mathrm{P(d)} < P_{start} \end{cases} \quad (2)$$

$$CDD(d) = \begin{cases} 0 & \mathrm{T(d)} \geq T_b,\ \mathrm{P(d)} < P_{start} \\ [T_b - T(d)]^x \times f[P(d)]^y & \mathrm{T(d)} < T_b,\ \mathrm{P(d)} < P_{start} \end{cases} \quad (3)$$

$$f[P(d)] = \frac{P(d)}{P_{start}} \quad (4)$$

where i$CDD(d)$ represents the accumulated coloring state. The cold temperatures below a limit T_b are accumulated when the day length becomes shorter than P_{start}. $P(d)$ and $T(d)$ represent the daily day length and mean temperature, respectively. $f[P(d)]$ is a function of $P(d)$, which suggests that photoperiods shorter than the P_{start} threshold may weaken the cold-degree effect. Two exponent indices x and y (take any of 0, 1, 2) are used to measure the possible effects of temperature and day length. The day length $P(d)$ depends on the day of the year (DOY) and latitude (L) (Forsythe et al., 1995).

The appearance of LCD (d) is recognized when $iCDD$ achieves a threshold Y_{crit}, given by:

$$iCDD(d) \geq Y_{crit} \quad (5)$$

The third autumn model was a spring-influenced autumn (SIA)

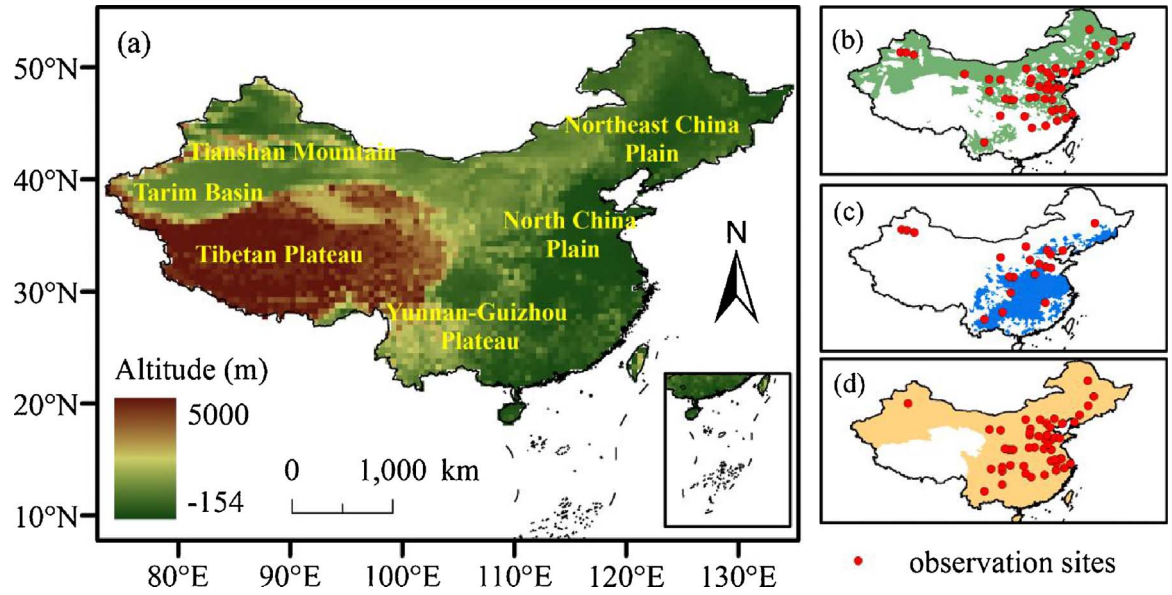

Fig. 1. Terrain (a) and distribution range of *U. pumila* (b), *F. chinensis* (c) and *R. pseudoacacia* (d) in China. The red circles represent the locations of phenological observation sites.

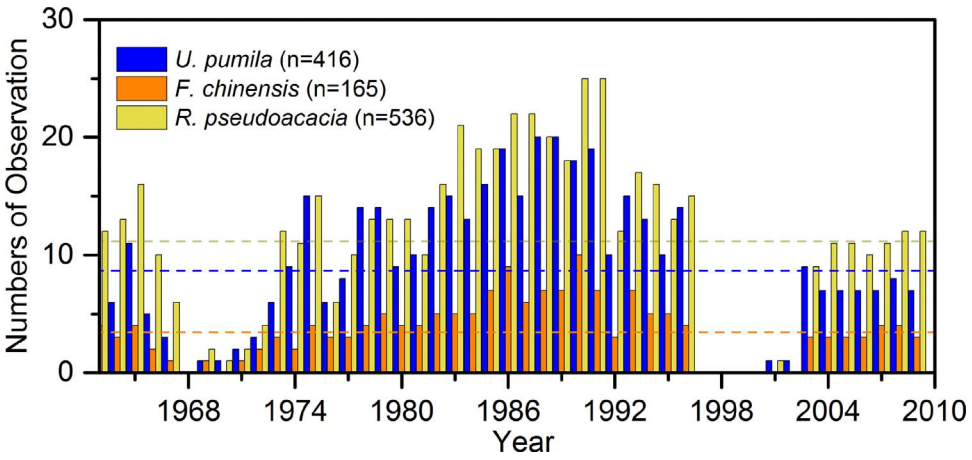

Fig. 2. Numbers of leaf coloring date (LCD) for *U. pumila*, *F. chinensis*, and *R. pseudoacacia* from 1963 to 2010. n: the total number of records. Dashed lines: average number of records per year.

model. The only difference between the SIA model and the TP model is that Y_{crit} is a linear function of the first leaf date (FLD) anomaly in the SIA model (Keenan and Richardson, 2015):

$$Y_{crit} = \alpha + \beta \times S_a \quad (6)$$

where α and β are parameters and S_a is the difference between FLD in the current year and the mean of all years.

To calibrate these models, we used the observation data in odd years and determined the parameter values by minimizing the sum of squared errors through a simulated annealing algorithm (Chuine et al., 1998). The remaining observation data were used for model validation. For the three autumn models, we compared their goodness of fit (r^2), mean absolute error (MAE), root mean square error (RMSE), model efficiency (ME), and statistical significance (p). We then applied the optimal autumn model and gridded temperature dataset to simulate the year-by-year LCD of each species across China during 1962–2012.

2.2.2. LCD changes along geographical gradients

Multiple regression analysis was used to examine the effect of geographical factors (i.e., latitude, longitude, and altitude) on mean LCD. The equation was:

$$LCD_{mean} = m_{lat} \times Lat + m_{lon} \times Lon + m_{alt} \times Alt + m_4 \quad (7)$$

where LCD_{mean} represents the mean LCD during 1962–2012. *Lat*, *Lon*, and *Alt* indicate the latitude, longitude, and altitude of the pixels, respectively. m_1, m_2, m_3 are the regression coefficients, and m_4 is a constant.

2.2.3. Spatial patterns of LCD variability

Empirical orthogonal function analysis was used to identify the most extensive and influential spatial modes of LCD variability and how they change with time (Ge et al., 2016). The EOFs were extracted by computing the eigenvalues and eigenvectors of a spatially weighted anomaly covariance matrix of the LCD. The derived eigenvalues suggested the percent variance explained by different modes. In this study, the eigenvalues represented how much the modes could explain LCD variability for three species. The time series or principal component (PC) of each mode was determined by projecting the derived eigenvectors onto the spatially weighted anomalies, which reflected the amplitude of each mode over the whole study period.

3. Results

3.1. Model fitting and validation

The fitted parameters of the MR model showed that the relationship between LCD and monthly temperature varied greatly between the species (Table 1). A temperature rise in May and June (positive

Table 1
Best-fitted parameters for three autumn phenology models: multiple regression (MR), temperature-photoperiod (TP), and spring-influenced autumn (SIA).

Model	Parameters	*U. pumila*	*F. chinensis*	*R. pseudoacacia*
MR	a	0.83	−0.69	0.14
	b	0.06	−1.75	0.77
	c	−0.36	−0.52	−0.10
	d	−0.63	2.41	−0.34
	e	4.51	4.41	2.66
	ε	227.37	212.41	240.02
TP	P_{start}	15.35	19.33	12.33
	T_b	14.42	19.76	29.17
	x	1	1	1
	y	0	0	2
	Y_{crit}	80.43	113.65	487.47
SIA	P_{start}	17.12	12.77	12.57
	T_b	13.44	20.95	29.75
	x	1	1	1
	y	1	0	0
	α	40.06	129.63	656.01
	β	0.46	−0.52	0.24

regression coefficient of T_5 and T_6) advanced the LCD of *F. chinensis*, but delayed the LCD of *U. pumila* and *R. pseudoacacia*. However, the LCD of all the three species exhibited positive correlation with the September temperature, indicating that a warmer September would result in a later LCD. Furthermore, the temperature in September had the strongest influence on the LCD of *U. pumila*, *F. chinensis* and *R. pseudoacacia* with a temperature sensitivity of 4.51, 4.41 and 2.66 days/°C, respectively.

The parameters of the TP and SIA models were also quite different among the species (Table 1). The photoperiod threshold (P_{start}) of *R. pseudoacacia* was apparently lower than that of other species, suggesting a relatively later beginning of the coloring process. The temperature had proportional effects ($x = 1$) on the LCD for all three species, but the effects of photoperiod were absent, proportional or more than proportional ($y = 0, 1, 2$) depending on species and model.

Regarding the internal validation (Fig. 3), the SIA model outperformed the other two models for *U. pumila* and *F. chinensis*, with r^2 of 0.64 and 0.51, MAE of 8.81 and 8.05 days, ME of 0.64 and 0.51, and RMSE of 11.73 and 10.45 days, respectively. For *R. pseudoacacia*, the MR model performed better than the SIA and TP models with r^2 of 0.37, MAE of 8.85, ME of 0.37, and RMSE of 10.89 days. The cross validation showed that the TP model gave the best simulation for LCD of *U. pumila* ($r^2 = 0.65$, MAE = 8.92 days, ME = 0.63, RMSE = 11.16 days). However, the most accurate models for *F. chinensis* and *R. pseudoacacia* were the MR model ($r^2 = 0.53$, MAE = 7.83 days, ME = 0.51, RMSE = 9.76 days) and the SIA model ($r^2 = 0.31$, MAE = 9.32 days, ME = 0.30, RMSE = 11.49 days), respectively. Since the cross-validation reflected the performance of the models in an independent condition, we determined the optimal models for the three species according to the results of cross-validation and applied them in the subsequent simulations.

3.2. Spatial patterns in mean LCD

By using the optimal models, the LCD of three species in each year was simulated. The mean LCD for the period 1963–2012 is shown in Fig. 4. For *U. pumila*, the mean LCD ranged from 188 to 365 DOY with a mean of 280.6 DOY. The earliest LCD occurred at the border area of the Tibetan Plateau in the south-west and Tianshan Mountains in the north-west. The latest LCD occurred in the North China Plain and Tarim Basin. The LCD of *F. chinensis* ranged from 211 to 321 DOY with a mean of 290.8 DOY and standard deviation (STD) of 19.1 days. It was later in the south-east compared to the north and west. The mean LCD of *R. pseudoacacia* was later than *U. pumila* and *F. chinensis* (mean: 296.8; STD: 12.7 days). The difference between the earliest and latest LCD of *R. pseudoacacia* was smaller (86 days) than the other two species. The earliest LCD of *R. pseudoacacia* occurred in the border area of the Tibetan Plateau in the south-west and Tianshan Mountain in the north-west, while the latest LCD occurred in south-east China.

The multiple regression models successfully reflected the relationship between mean LCD and geographical factors with r^2 ranging from 0.68 to 0.88 ($p < 0.01$) (Table 2). Latitude was negatively and significantly correlated with LCD for all three species ($p < 0.01$), with a 1° increase in latitude resulting in 3.19, 2.12 and 1.17 days advance in mean LCD for *U. pumila*, *F. chinensis* and *R. pseudoacacia*, respectively. The correlations between longitude and mean LCD were inconsistent among species. For *U. pumila* and *R. pseudoacacia*, the correlations were negative ($p < 0.01$) and the sensitivity of mean LCD to longitude reached −0.54 and −0.26 days/°, respectively. However, the mean LCD of *F. chinensis* presented positive correlations the longitude ($p < 0.05$), and the regression coefficient was relatively small (0.15 days/°). Altitude was also an important factor influencing the mean LCD. For a 100 m increase in altitude, the LCD of *U. pumila*, *F. chinensis* and *R. pseudoacacia* advanced by 3.04, 1.07 and 1.88 days, respectively.

3.3. Dominant EOF mode and associated time changes

The variances explained by the five leading EOF modes are listed in Table 3. The first and second EOF modes accounted for 30.02–48.94% and 11.31–18.38%, respectively, of the interannual variance in LCD of the three species. In addition, accumulated variances explained by the five leading EOF modes reached 62.64–78.74%. As the first two EOF modes together explained almost half of the variance, we just discussed the spatial pattern and associated time coefficients of these two modes.

For all the three species, the spatial pattern of LCD variability in the first EOF mode showed a homogeneous structure across China (Fig. 5a,c,e). Regarding *U. pumila*, the strongest EOF weights mainly concentrated in central parts of north China and north-west China, demonstrating that these areas had the strongest LCD variability. For *F. chinensis* and *R. pseudoacacia*, the EOF weights were stronger in south-east China compared with the other regions. The time coefficient of the first EOF mode (Fig. 6a,c,e) showed that the LCD of *U. pumila* and *R. pseudoacacia* was delayed by 1.25 days/decade and 0.53 days/decade ($p < 0.01$), respectively. The LCD of *F. chinensis* fluctuated greatly over the study period, and thus the delaying trend was weak (0.21 days/decade, $p > 0.05$).

The second EOF mode revealed clear regional differences (Fig. 5b,d,f). For *U. pumila*, the negative weights were distributed in north-west China and the North China Plain, while north-east China exhibited positive weights. For *F. chinensis* and *R. pseudoacacia*, there was an evident north-south effect, with the boundary around 30°N. This spatial pattern suggested that an earlier (later) LCD in the north was accompanied by a later (earlier) LCD in the south. The strongest weights were distributed in the south of the North China Plain for *F. chinensis*, and concentrated in south-east China and parts of north-east China for *R. pseudoacacia*. No significant trends were found in the time coefficient of the second EOF mode for any species (Fig. 6b,d,f). In addition, the interannual variations in the second EOF mode were smaller than those in the first EOF mode.

4. Discussion

In this study, three models were fitted for simulating the LCD of three tree species in China. Surprisingly, no single model gave the best fit for all species. In contrast, Keenan and Richardson (2015) found that the SIA model slightly outperformed the TP model when simulating the LCD of three species (*Fagus Grandifolia*, *Acer saccharum*, and *Betula alleghaniensis*) across the United States. However, the SIA model only displayed the best performance for *R. pseudoacacia* in China. It suggested that the applicability of the models might vary among different species and regions.

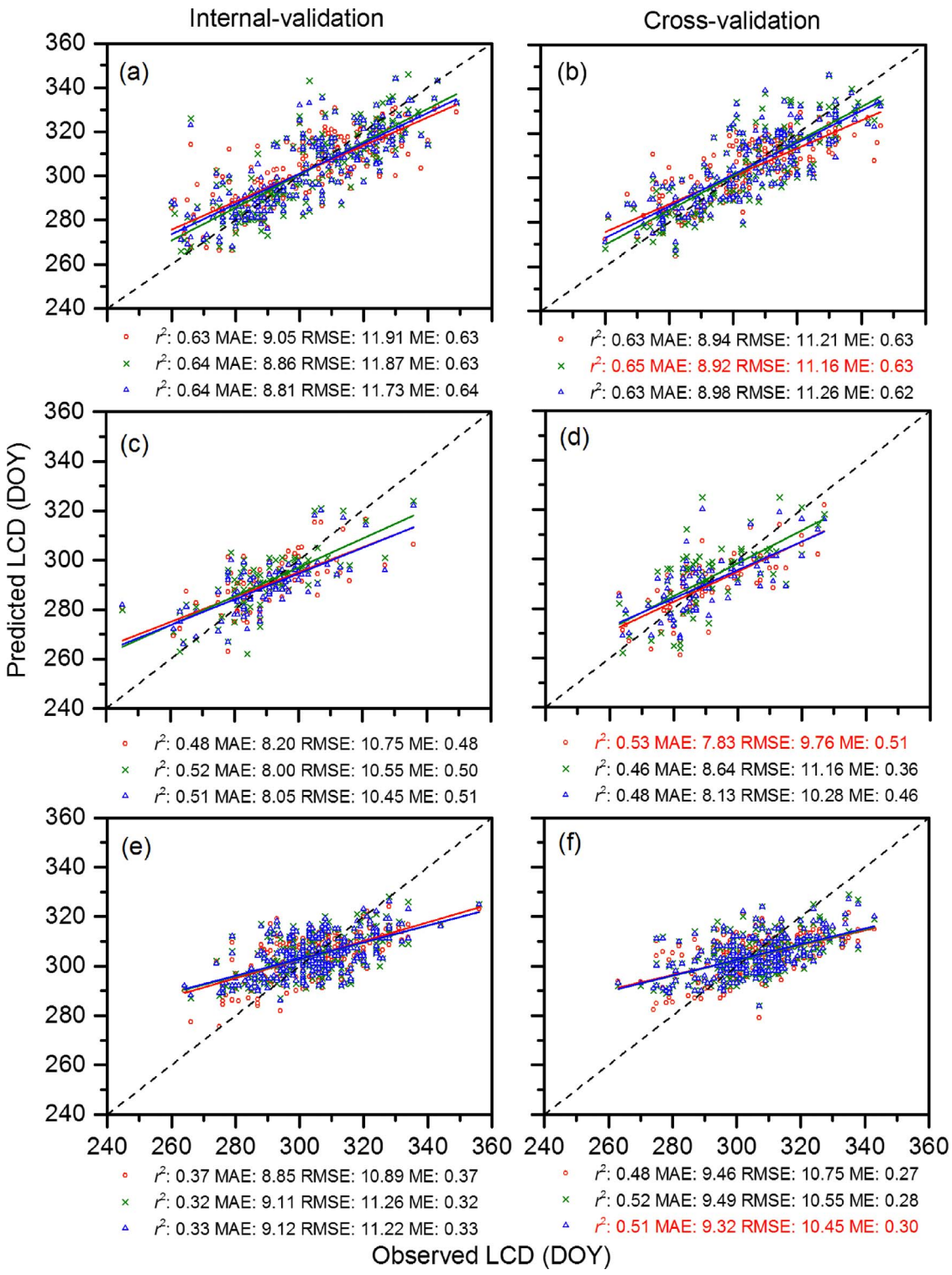

Fig. 3. Comparison of observed and predicted leaf coloring data (LCD) of *U. pumila* (a–b), *F. chinensis* (c–d) and *R. pseudoacacia* (e–f). The red circles, green crosses and blue triangles represent the results of the multiple regression (MR), temperature-photoperiod (TP) and spring-influenced autumn (SIA) model, respectively. The solid lines are linear regression plots. The red characters represent the statistics of the optimal model.

In agreement with previous studies (Dai et al., 2014; Liu et al., 2016b; Olsson and Jonsson, 2015), pre-season temperature (monthly mean temperature or accumulated cold temperature) exerted a significant influence on the LCD of all species. Compared with the temperature, the role of photoperiod was conflicting, Several studies have concluded that photoperiod is a powerful regulator of the progression of the autumn season, especially for long-lived, late successional species (Korner and Basler, 2010; Way and Montgomery, 2015). The leaf coloring time of seven species in the continental United States and two species in South Korea has been successfully simulated by the TP model (Jeong and Medvigy, 2014; Park et al., 2017). Both of those studies found that photoperiod not only determined the date when the cold temperature started to accumulate, but also impacted daily coloring state. However, in this study, the photoperiod showed little effect on

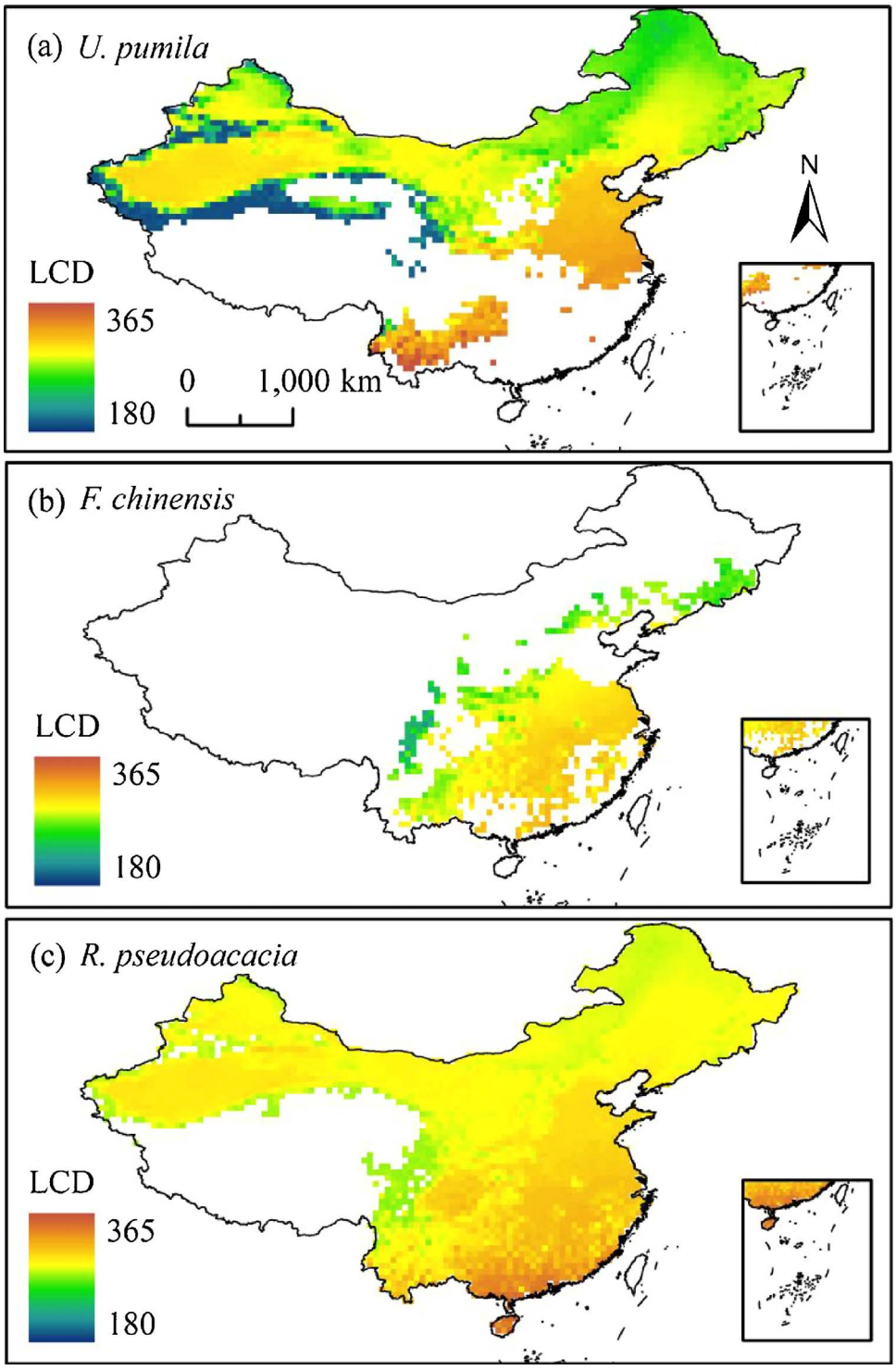

Fig. 4. Spatial patterns in mean leaf coloring date (LCD) of the three species during 1962–2012.

Table 2
Multiple regression analysis between mean leaf coloring date (LCD) of the three species and geographical factors.

Species	ε (d)	m_{lat} (d/°)	m_{lon} (d/°)	M_{alt} (d/100m)	r^2
U. pumila	502.51**	−3.19**	−0.54**	−3.04**	0.88**
F. chinensis	352.75**	−2.12**	0.15*	−1.70**	0.88**
R. pseudoacacia	384.85**	−1.17**	−0.26**	−1.88**	0.68**

**: $p < 0.01$, *: $p < 0.05$. The asterisks after r^2 indicate the significance of the regression models.

Table 3
Variance explained by the five leading empirical orthogonal function (EOF) modes.

Variance explanation	*U. pumila*	*F. chinensis*	*R. pseudoacacia*
EOF1	30.02%	46.95%	48.94%
EOF2	12.79%	18.38%	11.31%
EOF3	7.47%	8.56%	8.24%
EOF4	7.30%	6.72%	5.65%
EOF5	5.06%	4.12%	4.60%
Sum	62.64%	84.73%	78.74%

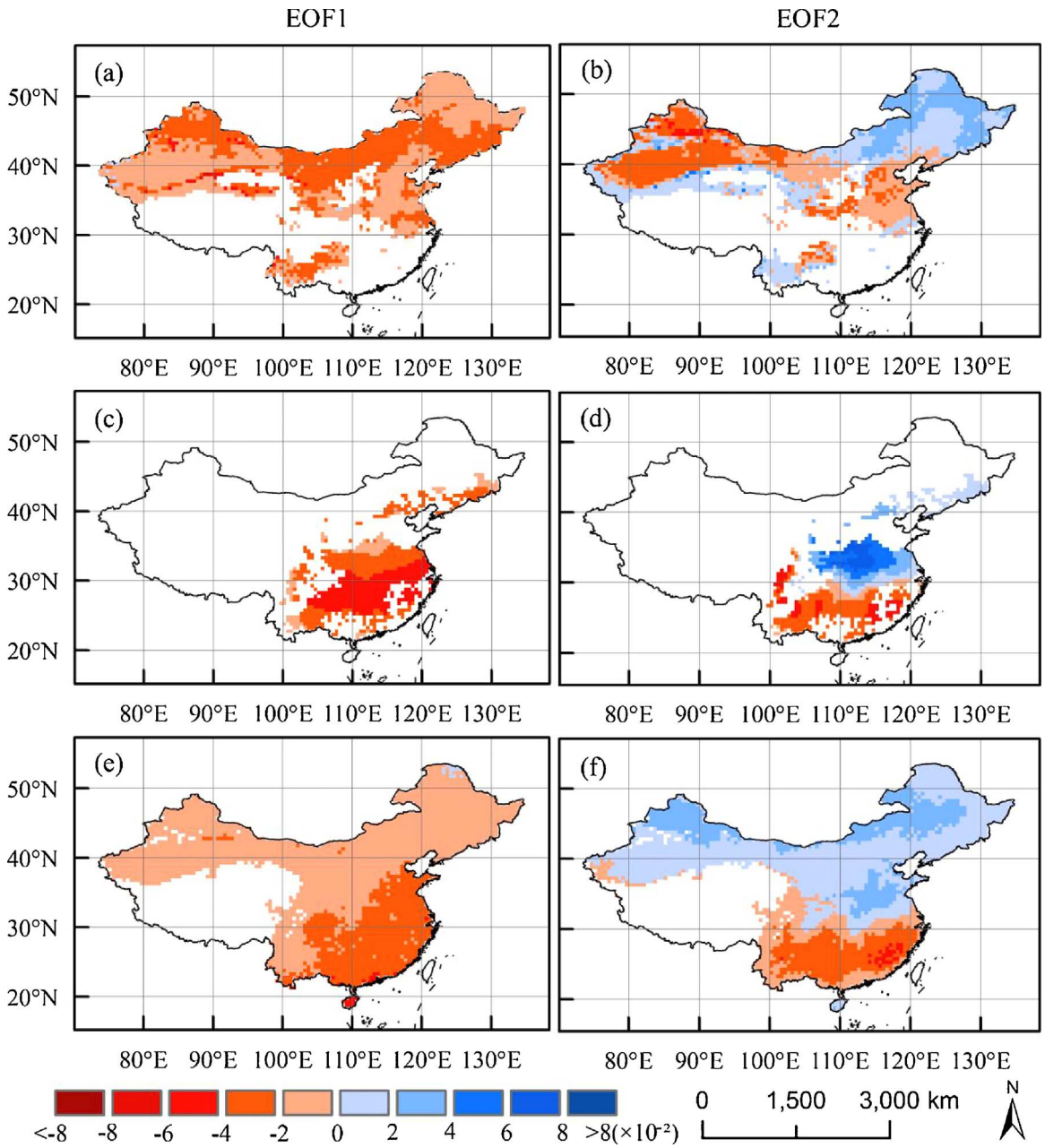

Fig. 5. Spatial pattern of the two leading empirical orthogonal function (EOF) modes in leaf coloring date (LCD) of (a,b) *U. pumila*, (c,d) *F. chinensis* and (e,f) *R. pseudoacacia*, 1962–2012.

daily coloring state for *U. pumila* and *R. pseudoacacia*, which is consistent with the model for simulating LCD of *Quercus* sp. in France (Delpierre et al., 2009). With regard to *F. chinensis*, the MR model, which did not consider the impact of photoperiod, performed the best among the three models. Meanwhile, through $y = 0$, even the TP and SIA model also demonstrated that the photoperiod had no influence on daily coloring state of *F. chinensis*. Thus, we could conclude that the role of photoperiod varied among species and regions. In previous studies, a stronger response of autumn phenology to accumulated cold-degree days was found at latitudes with less severe winters (Dragoni and Rahman, 2012). In these areas, photoperiodic regulation can be expected to be relatively weaker (Estiarte and Penuelas, 2015). This could partly explain why *F. chinensis*, which is mainly distributed at lower latitudes around 20–40 N°, did not respond to the photoperiod in autumn in the present study.

Overall, the mechanism of autumn phenology is still poorly understood, which hinders accurate parameterization of the phenological process in autumn (Basler, 2016). The optimal autumn models in this study showed relatively lower predictive power (RMSE = 9.76–11.49 days) than the spring phenology models studied elsewhere (RMSE = 2–6 days for site-specific predictions and 7–9 days for multiple sites prediction) (Basler, 2016; Linkosalo et al., 2006). A few studies have tested other forms of temperature parameters, such as growing degree-days (Olsson and Jonsson, 2015; Wallman et al., 2005) or critical threshold of daily average temperature (Foley et al., 1996), to describe the relationship between autumn phenology and climate. However, none of those assumed models exhibited better performance than the models using cold degree days. On the one hand, the uncertainties in autumn models are caused by phenological observations. Compared with spring phenophases, autumn phenophases are more difficult to identify and can easily be influenced by unpredictable weather, such as wind and rainfall (Delpierre et al., 2009). The advances in digital camera technology in recent years may help monitor plant dynamics in autumn accurately. (Petach et al., 2014; Klosterman

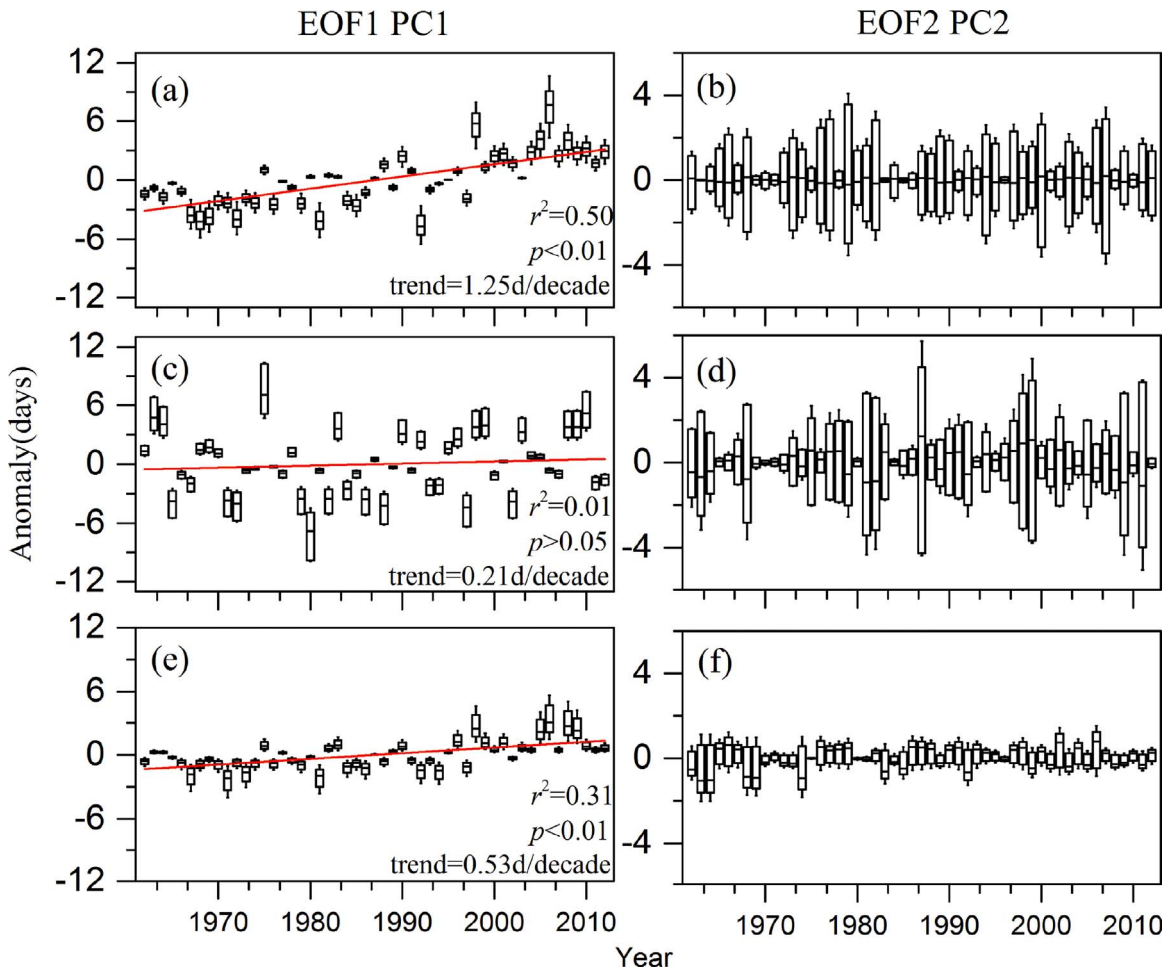

Fig. 6. Boxplot of principal component (PC) time series of empirical orthogonal function (EOF) modes for leaf coloring date (LCD) of *U. pumila* (a,b), *F. chinensis* (c,d) and *R. pseudoacacia* (e,f), 1962–2012. All PC values are scaled to anomalies in days by multiplying the mean value of EOF weights in Fig. 5. The lines show the linear regression line. The bottoms and tops of the boxes are the 25th and 75th percentiles, respectively. The bands in the boxes show the median value of anomalies. The ends of the whiskers indicate the standard deviation.

et al., 2014; Nasahara and Nagai, 2015). On the other hand, the drivers of leaf coloring are seldom tested in controlled experiments. The effects of precipitation and biotic factors (e.g., pathogens) have never been examined and considered in autumn phenological models. In the future, more experiments concerning autumn phenology are needed.

Regarding the spatial modes of LCD variability, the first EOF mode, which accounted for 30.02–48.94% of the variation, revealed a consistent advance or delay in the LCD across space. This intraspecific synchrony in phenological change has also been found in northern Australia (Franklin and Bach, 2006) and western Poland (Sparks et al., 2012). However, the second EOF mode suggested reverse trends between north and south for *F. chinensis* and *R. pseudoacacia*. This spatial pattern of LCD variations may be caused by differences in the magnitude or direction of temperature shifts. For instance, Ge et al. (2015) analyzed the temperature trends from September to November across China over the past 50 years and found a stronger warming trend in the north than in the south. A similar conclusion has also been drawn on hemisphere-scale (Jones et al., 2012).

5. Conclusions

This study systematically tested autumn phenology models using LCD time series of several typical tree species at more than 50 sites across China. The findings demonstrated that (1) no single model gave the best fit for all the three species. The LCD of *F. chinensis* was only determined by pre-season temperature, while the LCD of *U. pumila* and *R. pseudoacacia* was better fitted to the TP and SIA models, which consider both the effect of temperature and photoperiod. (2) The simulated mean LCD of *U. pumila*, *F. chinensis* and *R. pseudoacacia* was October 6, October 16, and October 22, respectively. The latitude, longitude, and altitude had a significant influence on the mean LCD, but the direction of change in LCD along longitude was inconsistent among species. (3) The first EOF mode presented a homogeneous structure across China for all the three species. The second EOF mode exhibited opposite weights in north and south for *F. chinensis* and *R. pseudoacacia*. As manifested by the PC time series of the first EOF mode, the LCD of all three species was delayed at a rate of 1.25, 0.21 and 0.53 days/decade for *U. pumila*, *F. chinensis,* and *R. pseudoacacia*, respectively.

Acknowledgements

This work was funded by National Natural Science Foundation of China (Grant No. 41427805), Key Programs of the Chinese Academy of Sciences (Grant No. KFZD-SW-310), and National Natural Science Foundation of China (Grant No. 41601047).

Appendix A. Supplementary data

Supplementary data associated with this article can be found, in the online version, at http://dx.doi.org/10.1016/j.agrformet.2017.10.034.

References

Aono, Y., Omoto, Y., 1990. Estimation of blooming date for prunus yedoensis using DTS

combined with Chil-unit accumulations. J. Agric. Meteorol. 45 (4), 243–249.
Basler, D., 2016. Evaluating phenological models for the prediction of leaf-out dates in six temperate tree species across central Europe. Agric. For. Meteorol. 217, 10–21.
Bluemel, K., Chmielewski, F.-M., 2012. Shortcomings of classical phenological forcing models and a way to overcome them. Agric. For. Meteorol. 164 (8), 10–19.
Chen, X., Xu, L., 2012. Phenological responses of Ulmus pumila (Siberian Elm) to climate change in the temperate zone of China. Int. J. Biometeorol. 56 (4), 695–706.
Chuine, I., Cour, P., Rousseau, D.D., 1998. Fitting models predicting dates of flowering of temperate-zone trees using simulated annealing. Plant Cell Environ. 21 (5), 455–466.
Chuine, I., 2000. A unified model for budburst of trees. J. Theor. Biol. 207 (3), 337–347.
Cleland, E.E., Chuine, I., Menzel, A., Mooney, H.A., Schwartz, M.D., 2007. Shifting plant phenology in response to global change. Trends Ecol. Evol. 22 (7), 357–365.
Dai, J.H., Wang, H.J., Ge, Q.S., 2014. The spatial pattern of leaf phenology and its response to climate change in China. Int. J. Biometeorol. 58 (4), 521–528.
Delpierre, N., et al., 2009. Modelling interannual and spatial variability of leaf senescence for three deciduous tree species in France. Agric. For. Meteorol. 149 (6–7), 938–948.
Dragoni, D., Rahman, A.F., 2012. Trends in fall phenology across the deciduous forests of the Eastern USA. Agric. For. Meteorol. 157, 96–105.
Estiarte, M., Penuelas, J., 2015. Alteration of the phenology of leaf senescence and fall in winter deciduous species by climate change: effects on nutrient proficiency. Global Change Biol. 21 (3), 1005–1017.
Estrella, N., Menzel, A., 2006. Responses of leaf colouring in four deciduous tree species to climate and weather in Germany. Clim. Res. 32 (3), 253–267.
Fang, J., Wang, Z., Tang, Z., 2009. Atlas of Woody Plants in China. Higher Education Press, Beijing.
Foley, J.A., et al., 1996. An integrated biosphere model of land surface processes, terrestrial carbon balance, and vegetation dynamics. Global Biogeochem. Cy 10 (4), 603–628.
Forsythe, W.C., Rykiel, E.J., Stahl, R.S., Wu, H.I., Schoolfield, R.M., 1995. A model comparison for daylength as a function of latitude and day of year. Ecol. Model. 80 (1), 87–95.
Fracheboud, Y., et al., 2009. The control of autumn senescence in European Aspen. Plant Physiol. 149 (4), 1982–1991.
Franklin, D.C., Bach, C.S., 2006. Assessing intraspecific phenological synchrony in zoochorous trees from the monsoon forests of northern Australia. J. Trop. Ecol. 22 (4), 419–429.
Fu, Y.S.H., et al., 2014. Variation in leaf flushing date influences autumnal senescence and next year's flushing date in two temperate tree species. P. Natl. Acad. Sci. U. S. A. 111 (20), 7355–7360.
Garonna, I., et al., 2014. Strong contribution of autumn phenology to changes in satellite-derived growing season length estimates across Europe (1982–2011). Global Change Biol. 20 (11), 3457–3470.
Ge, Q., Zhang, X., Zheng, J., 2014a. Simulated effects of vegetation increase/decrease on temperature changes from 1982 to 2000 across the Eastern China. Int. J. Climatol. 34 (1), 187–196.
Ge, Q.S., Wang, H.J., Dai, J.H., 2014b. Simulating changes in the leaf unfolding time of 20 plant species in China over the twenty-first century. Int. J. Biometeorol. 58 (4), 473–484.
Ge, Q.S., Wang, H.J., Rutishauser, T., Dai, J.H., 2015. Phenological response to climate change in China: a meta-analysis. Global Change Biol. 21 (1), 265–274.
Ge, Q.S., Dai, J.H., Cui, H.J., Wang, H.J., 2016. Spatiotemporal variability in start and end of growing season in China related to climate variability. Remote Sens. 8 (5).
Gill, A.L., et al., 2015. Changes in autumn senescence in northern hemisphere deciduous trees: a meta-analysis of autumn phenology studies. Ann. Bot-London 116 (6), 875–888.
Jeong, S.J., Medvigy, D., 2014. Macroscale prediction of autumn leaf coloration throughout the continental United States. Global Ecol. Biogeogr. 23 (11), 1245–1254.
Jeong, S.-J., Medvigy, D., Shevliakova, E., Malyshev, S., 2013. Predicting changes in temperate forest budburst using continental-scale observations and models. Geophys. Res. Lett. 40 (2), 359–364.
Jones, P.D., et al., 2012. Hemispheric and large-scale land-surface air temperature variations: an extensive revision and an update to 2010. J. Geophys. Res-Atmos. 117 (D5) (n/a-n/a).
Keenan, T.F., Richardson, A.D., 2015. The timing of autumn senescence is affected by the timing of spring phenology: implications for predictive models. Global Change Biol. 21 (7), 2634–2641.
Klosterman, S.T., et al., 2014. Evaluating remote sensing of deciduous forest phenology at multiple spatial scales using PhenoCam imagery. Biogeosciences 11 (16), 4305–4320.
Korner, C., Basler, D., 2010. Phenology under global warming. Science 327 (5972), 1461–1462.
Lim, P.O., Kim, H.J., Nam, H.G., 2007. Leaf senescence. Annu. Rev. Plant Biol. 58, 115–136.
Linkosalo, T., Häkkinen, R., Hänninen, H., 2006. Models of the spring phenology of boreal and temperate trees: is there something missing? Tree Physiol. 26 (9), 1165–1172.
Liu, Q., et al., 2016a. Delayed autumn phenology in the Northern Hemisphere is related to change in both climate and spring phenology. Global Change Biol. 22 (11), 3702–3711.
Liu, Q., et al., 2016b. Temperature, precipitation, and insolation effects on autumn vegetation phenology in temperate China. Global Change Biol. 22 (2), 644–655.
Menzel, A., 2003. Plant phenological anomalies in Germany and their relation to air temperature and NAO. Clim. Change 57 (3), 243–263.
Nasahara, K.N., Nagai, S., 2015. Review: development of an in situ observation network for terrestrial ecological remote sensing: the Phenological Eyes Network (PEN). Ecol. Res. 30 (2), 211–223.
Olsson, C., Jonsson, A.M., 2015. A model framework for tree leaf colouring in Europe. Ecol. Model. 316, 41–51.
Park, C.-K., Ho, C.-H., Jeong, S.-J., Lee, E.J., Kim, J., 2017. Spatial and temporal changes in leaf coloring date of Acer palmatum and Ginkgo biloba in response to temperature increases in South Korea. PLoS One 12 (3), 1–18.
Petach, A.R., Toomey, M., Aubrecht, D.M., Richardson, A.D., 2014. Monitoring vegetation phenology using an infrared-enabled security camera. Agric. For. Meteorol. 195, 143–151.
Richardson, A.D., et al., 2013. Climate change, phenology, and phenological control of vegetation feedbacks to the climate system. Agric. For. Meteorol. 169 (3), 156–173.
Solla, A., Martin, J.A., Corral, P., Gil, L., 2005. Seasonal changes in wood formation of Ulmus pumila and U-minor and its relation with Dutch elm disease. New Phytol. 166 (3), 1025–1034.
Sparks, T.H., Mizera, T., Wójtowicz, W., Tryjanowski, P., 2012. Synchrony in the phenology of a culturally iconic spring flower. Int. J. Biometeorol. 56 (2), 407–409.
Visser, M.E., 2016. Phenology: interactions of climate change and species. Nature 535 (7611), 236–237.
Wallman, P., Svensson, M.G.E., Sverdrup, H., Belyazid, S., 2005. ForSAFE—an integrated process-oriented forest model for long-term sustainability assessments. For. Ecol. Manage. 207 (1–2), 19–36.
Way, D.A., Montgomery, R.A., 2015. Photoperiod constraints on tree phenology, performance and migration in a warming world. Plant Cell Environ. 38 (9), 1725–1736.
Wu, Z., Raven, P.H., Hong, D., 1994. Flora of China. Science Press, Beijing.
Wu, C., Gough, C.M., Chen, J.M., Gonsamo, A., 2013. Evidence of autumn phenology control on annual net ecosystem productivity in two temperate deciduous forests. Ecol. Eng. 60, 88–95.
Xin, Q.C., 2016. A risk-benefit model to simulate vegetation spring onset in response to multi-decadal climate variability: theoretical basis and applications from the field to the Northern Hemisphere. Agric. For. Meteorol. 228, 139–163.
Yu, R., Schwartz, M.D., Donnelly, A., Liang, L., 2016. An observation-based progression modeling approach to spring and autumn deciduous tree phenology. Int. J. Biometeorol. 60 (3), 335–349.
Zu, J.X., Yang, J., 2016. Temporal variation of vegetation phenology in northeastern China (in Chinese). Acta Ecol. Sin. 36 (7), 2015–2023.